Joint inversion of Rayleigh wave phase velocity and ellipticity using USArray: Constraining velocity and density structure in the upper crust

Fan-Chi Lin,[1] Brandon Schmandt,[1] and Victor C. Tsai[1]

Received 27 April 2012; revised 22 May 2012; accepted 23 May 2012; published 21 June 2012.

[1] Rayleigh wave ellipticity, or H/V ratio, observed on the surface is particularly sensitive to shallow earth structure. In this study, we jointly invert measurements of Rayleigh wave H/V ratio and phase velocity between 24–100 and 8–100 sec period, respectively, for crust and upper mantle structure beneath more than 1000 USArray stations covering the western United States. Upper crustal structure, in particular, is better constrained by the joint inversion compared to inversions based on phase velocities alone. In addition to imaging Vs structure, we show that the joint inversion can be used to constrain Vp/Vs and density in the upper crust. New images of uppermost crustal structure (<3 km depth) are in excellent agreement with known surface features, with pronounced low Vs, low density, and high Vp/Vs anomalies imaged in the locations of several major sedimentary basins including the Williston, Powder River, Green River, Denver, and San Juan basins. These results demonstrate not only the consistency of broadband H/V ratios and phase velocity measurements, but also that their complementary sensitivities have the potential to resolve density and Vp/Vs variations. **Citation:** Lin, F.-C., B. Schmandt, and V. C. Tsai (2012), Joint inversion of Rayleigh wave phase velocity and ellipticity using USArray: Constraining velocity and density structure in the upper crust, *Geophys. Res. Lett.*, *39*, L12303, doi:10.1029/2012GL052196.

1. Introduction

[2] The deployment of EarthScope's USArray has facilitated the development of new methods to study detailed earth structure. Recent advances in both ambient noise surface-wave tomography [e.g., *Bensen et al.*, 2007; *Lin et al.*, 2009] and earthquake based surface-wave tomography [e.g., *Pollitz and Snoke*, 2010; *Lin and Ritzwoller*, 2011] provide exceptionally high-resolution images of isotropic and anisotropic structure in the crust and upper mantle of the western U.S. [e.g., *Moschetti et al.*, 2010; *Lin et al.*, 2011]. These studies use surface-wave traveltime and amplitude measurements from broadband USArray data to first invert for two dimensional (2D) surface wave properties such as phase velocity and azimuthal anisotropy at each station location for a range of periods. Dispersion properties are then used to invert for depth dependent structure. A limitation on the geological and seismological utility of the resulting models is that they provide only weak constraints on uppermost crustal structure (<3 km) because the limited period range (8–100 sec) of high quality dispersion measurements results in strong tradeoffs between shear velocity parameters at different depths. Improved imaging of upper crustal structure would aid in efforts to understand the relationship between geologic observations at the surface and deep crustal processes. Additionally, constraints on strongly heterogeneous upper crustal structure help to mitigate artifacts in studies of deeper 3D velocity structure [*Waldhauser et al.*, 2002; *Bozdağ and Trampert*, 2008] and lithospheric discontinuities [*Langston*, 2011], and allow for more accurate prediction of earthquake ground motions [*Vidale and Helmberger*, 1988].

[3] Rayleigh wave ellipticity, or the Rayleigh wave H/V (horizontal to vertical) ratio, has long been known to be particularly sensitive to shallow earth structure [e.g., *Boore and Nafi Toksöz*, 1969]. The microtremor H/V ratio (>1 Hz), which is often linked to the Rayleigh wave H/V ratio, has been widely used to characterize site response, predict ground motion, and invert for velocity in the top several hundred meters [e.g., *Nakamura*, 1989; *Fäh et al.*, 2001]. These studies analyze the horizontal to vertical spectral ratio of observed ambient noise, although the physical origin of this signal is somewhat ambiguous because it depends on the contents of noise signals: i.e., whether they are predominately fundamental mode Rayleigh waves, predominately body waves, or a mixture of different wave types (see *Bonnefoy-Claudet et al.* [2006] for review). Long period (>20 sec) Rayleigh H/V ratio studies based on earthquake signals [e.g., *Tanimoto and Rivera*, 2008; *Yano et al.*, 2009] are theoretically more straightforward to understand, but are relatively less common. This is potentially due to the traditionally sparse broadband station distribution for large-scale studies and the uncertainty regarding whether long-period H/V ratio measurements are robust and compatible with traditional phase and group velocity measurements [*Ferreira and Woodhouse*, 2007].

[4] In this study, the Rayleigh wave H/V ratio is measured for more than 1000 USArray stations in the western U.S. for periods between 24 and 100 sec using teleseismic events. We show that the H/V ratio measurements are consistent with ambient noise and earthquake based phase velocity measurements between 8 and 100 sec period [*Lin et al.*, 2009; *Lin and Ritzwoller*, 2011], and that these measurements add complementary constraints to inversions for 3D structure. Upper crustal structure, in particular, is better resolved. We image prominent low Vs anomalies in the

[1]Seismological Laboratory, Division of Geological and Planetary Sciences, California Institute of Technology, Pasadena, California, USA.

Corresponding author: F.-C. Lin, Seismological Laboratory, Division of Geological and Planetary Sciences, California Institute of Technology, 1200 E. California Blvd., MS 252-21, Pasadena, CA 91125, USA. (linf@caltech.edu)

©2012. American Geophysical Union. All Rights Reserved.

upper 3 km that were not recovered by prior inversions, but are well correlated with major sedimentary basins known from resource exploration studies [*Blackwell et al.*, 2006]. Moreover, we show that the complementary sensitivities of H/V ratio and phase velocity facilitate simultaneous inversion for Vs, Vp/Vs, and density in the upper crust.

2. Data and Results

[5] More than 900 earthquakes with Ms > 5.0 between 2007 January 1 and 2011 June 30 are used in this study. For each earthquake and each available station, we apply automated frequency-time analysis (FTAN) [*Bensen et al.*, 2007] to determine Rayleigh wave traveltimes and amplitudes in both the vertical and radial components and the vertical (V) and radial (H) amplitude ratio is used to evaluate the H/V ratios between 24 and 100 sec period at the station location. Here, because the radial component is well defined by the direction of wave propagation (determined by the gradient of the Rayleigh wave phase traveltime surface [*Lin and Ritzwoller*, 2011]), different from traditional H/V ratio analysis based on microtremor signals [*Bonnefoy-Claudet et al.*, 2006], we can simply interpret the observed H/V ratio in terms of Rayleigh wave ellipticity.

[6] To include only the most reliable measurements and avoid potential bias due to wave complexities (e.g., wave interference), several selection criteria are imposed. First, measurements with signal-to-noise ratio smaller than 10 (SNR) [*Bensen et al.*, 2007] in the vertical component are removed from further analysis. Second, we impose additional selection criterion based on the vertical and radial phase difference [*Tanimoto and Rivera*, 2008] and remove all measurements with $|\tau_R-\tau_V-T/4| > 10$ sec, where τ_R and τ_V are the radial and vertical phase traveltime and T is the period. While this 10-sec criterion is easier to satisfy for short period measurements (<30 s), fewer short-period measurements pass the first selection criterion. Third, considering the reasonable range of the H/V ratio in the period band we investigated [*Tanimoto and Rivera*, 2008], we remove obvious outliers with H/V ratio >2. The number of measurements removed by the third criterion is in general small, however.

[7] For each period and station, all available H/V measurements from different earthquakes are statistically summarized, where the mean and the standard deviation of the mean are used to estimate the H/V ratio and its uncertainty at the station location. Although the H/V ratio is, in theory, sensitive to azimuthal anisotropy and can be directionally dependent, initial inspection suggests that measurements are too scattered for such study and all measurements from different directions are treated equally in this study. As an additional quality control, we remove all H/V ratio measurements outside the 2σ range (Figure S1 in the auxiliary material), even though this results in a slight underestimate of the true range of values.[1] Figures 1a and 1b show the results of the estimated H/V ratio at 30 and 60 sec periods. In order to facilitate a joint inversion with Rayleigh wave phase velocity measurements (e.g., Figures 1c and 1d), we interpolate the results onto a 0.2° by 0.2° grid by applying 0.5° Gaussian smoothing. The phase velocity measurements used in this study are derived from earlier tomography studies based on ambient noise (8–24 sec [*Lin et al.*, 2009]) and teleseismic earthquakes (24–100 sec [*Lin and Ritzwoller*, 2011]) with data updated to 2011 June 30. The depth sensitivity kernels of H/V ratio and phase velocity to Vs, Vp, and density perturbations are also shown for reference. The kernels shown here are for illustration only and are calculated based on the 1D PREM model [*Dziewonski and Anderson*, 1981].

[8] Clear correlation is observed between the observed H/V ratios and known geological features at both 30 and 60 sec periods (Figures 1a and 1b). More specifically, high H/V ratios are observed in major sedimentary basins (e.g., the Williston Basin near eastern Montana and western North Dakota) and low H/V ratios are observed in major mountain ranges (e.g., the southern Rockies in Colorado). This contrast is to be expected as a result of large differences in the elastic properties of sediments and crystalline bedrock. Unlike Rayleigh wave phase velocity, which has peak sensitivity to Vs structure at a depth near a third of its wavelength (Figures 1c and 1d), sensitivity of the H/V ratio to Vs structure is maximal in the upper few km even for long periods (Figure 1b). However, non-zero Vs sensitivity does penetrate into the mantle at longer periods and the sign of Vs sensitivity is reversed (Figure 1b). Consequently, at a period of 60 sec, the map of H/V ratio is positively correlated with well known features of upper mantle velocity structure, with low values in the region of the Snake River Plain/Yellowstone hotspot track and a clear long-wavelength dichotomy between the western Cordillera and the tectonically stable interior (Figure 1d).

[9] To demonstrate the consistency of the Rayleigh wave H/V ratio and phase velocity measurements and how the H/V ratio can be used to provide additional constraints on Earth structure, we perform three different inversions for 1-D structure in the depth range of 0–250 km beneath each location. The three inversions are only different in how each model parameter is allowed to vary and whether the H/V ratio is used as a constraint. In the first two inversions (Model 1&2), we fix the density (ρ) and Vp/Vs profiles to the reference model (see Table S1) and only Vs is allowed to vary. Only phase velocity measurements are used as constraints in Model 1, while phase velocity and H/V ratio are jointly inverted in Model 2. In the third inversion (Model 3), we jointly inverted the two measurements and in additional to the Vs profile, both density (ρ) and Vp/Vs are allowed to change in the upper crust. Similar to Moschetti et al. 2010, the model is parameterized by four crustal layers and five mantle cubic B-splines (see Table S1 for model parameters). In each inversion, we iteratively calculate the depth sensitivity kernels [*Herrmann and Ammon*, 2002] and perturb the model parameters in the steepest descent direction until the misfit between observed and predicted dispersion quantities is minimized. The initial models for the three inversions are the reference model (Table S1), model 1, and model 2 respectively. To illustrate the differences between the three inversions, we present the results of each for a location in the Williston Basin (Figures 2a–2e). For each inversion, the compilation of all the inverted 1-D profiles is then used to determine the 3D model (Model 1–3).

[10] At the example location, Model 1 (no H/V ratio constraints) accurately fits the phase velocity measurements (Figures 2a and 2c), but there is a significant offset between

[1]Auxiliary materials are available in the HTML. doi:10.1029/2012GL052196.

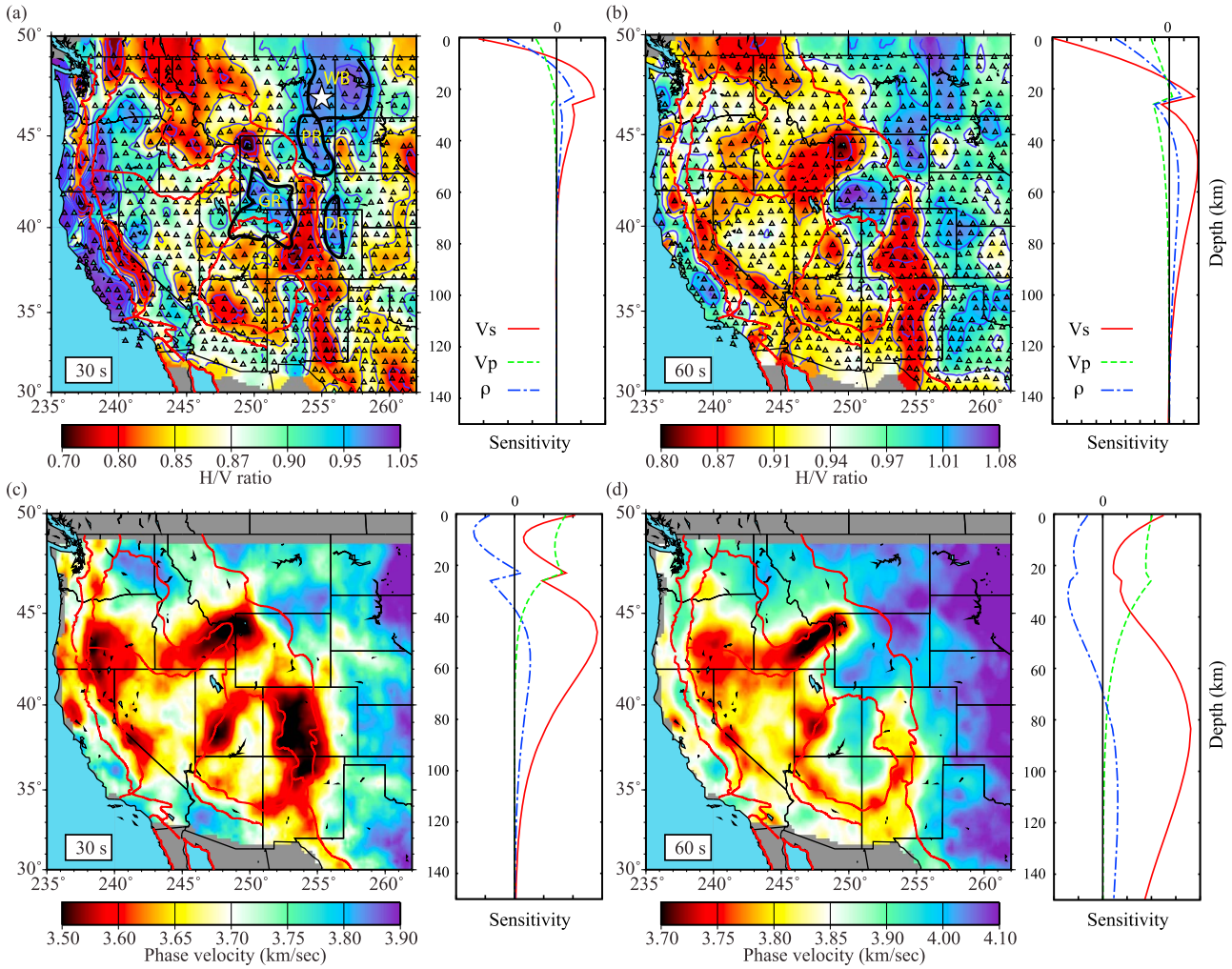

Figure 1. (a) The 30 sec Rayleigh wave H/V ratio observed across the USArray. The triangles denote the stations used in this study and the star indicates the example location used in Figures 2 and 4. The 3 km sediment contours are also shown for several major sedimentary basins mentioned in the text [*Blackwell et al.*, 2006]; WB: Williston Basin; PR: Powder River Basin; GR: Green River Basin; DB: Denver Basin). The depth sensitivities of 30 sec H/V ratio to Vs, density (ρ), and Vp/Vs perturbation are shown in the right. (b) Same as Figure 1a but for 60 sec H/V ratio. (c, d) Same as Figures 1a and 1b but for Rayleigh wave phase velocity.

the predicted and observed H/V ratios (Figure 2b). The Williston Basin provides a useful test case for evaluating subsequent inversions including the H/V ratio because it is known to have a total sedimentary thickness of ~3 km, with weakly consolidated sediments in the upper few hundred meters underlain by multiple sedimentary strata of Ordovician to Cretaceous ages [*Blackwell et al.*, 2006; *Gerhard et al.*, 1982]. Active source refraction data are consistent with an average Vp of ~3.5 km/s for the sedimentary layer [*Hajnal et al.*, 1984; *Morel-a-l'Huissier et al.*, 1987], though high-frequency wellbore data show that distinct sedimentary units exhibit large variations [e.g., *Spikes*, 2011]. Using a reasonable range of sedimentary Vp/Vs values (1.65–2 [*Mavko et al.*, 1998]) implies a Vs of 1.75–2.12 km/s for the upper 3 km, whereas Model 1 finds a much higher value of 3 km/s. Model 1 does show more pronounced low Vs anomalies in other basins (e.g., the Green River Basin in southwest Wyoming; Figure 3a), but the inversion with only phase velocities appears to be limited to resolving basins where sediment thickness is greater than ~5 km [*Blackwell et al.*, 2006], and even in those locations sediment velocities are likely overestimated. In more dense arrays where high quality phase velocity measurements can be made at periods shorter than 8 sec, inversions using only phase velocity can achieve higher resolution in the upper 3 km [e.g., *Yang et al.*, 2011].

[11] In Model 2, while again only the Vs profile is allowed to vary, we weight the period-averaged phase velocity misfit (χ^2_c) and H/V ratio misfit ($\chi^2_{H/V}$) equally and minimize the overall misfit ($\chi^2 = (\chi^2_c + \chi^2_{H/V}) / 2$). In general, the H/V ratios are better predicted and the predicted phase velocities still agree well with the observations (e.g., Figures 2a and 2b). This suggests that the H/V ratio measurements provide additional constraints on the inverted model. At the example location, Model 2 has a ~1 km/s velocity drop compared to Model 1 in the uppermost layer (Figure 2c) placing it in good agreement with resource exploration studies. Despite the significant reduction of the offset, clear deviation does remain between the predicted and observed H/V ratios at long periods (>30 sec) suggesting that varying only Vs is not

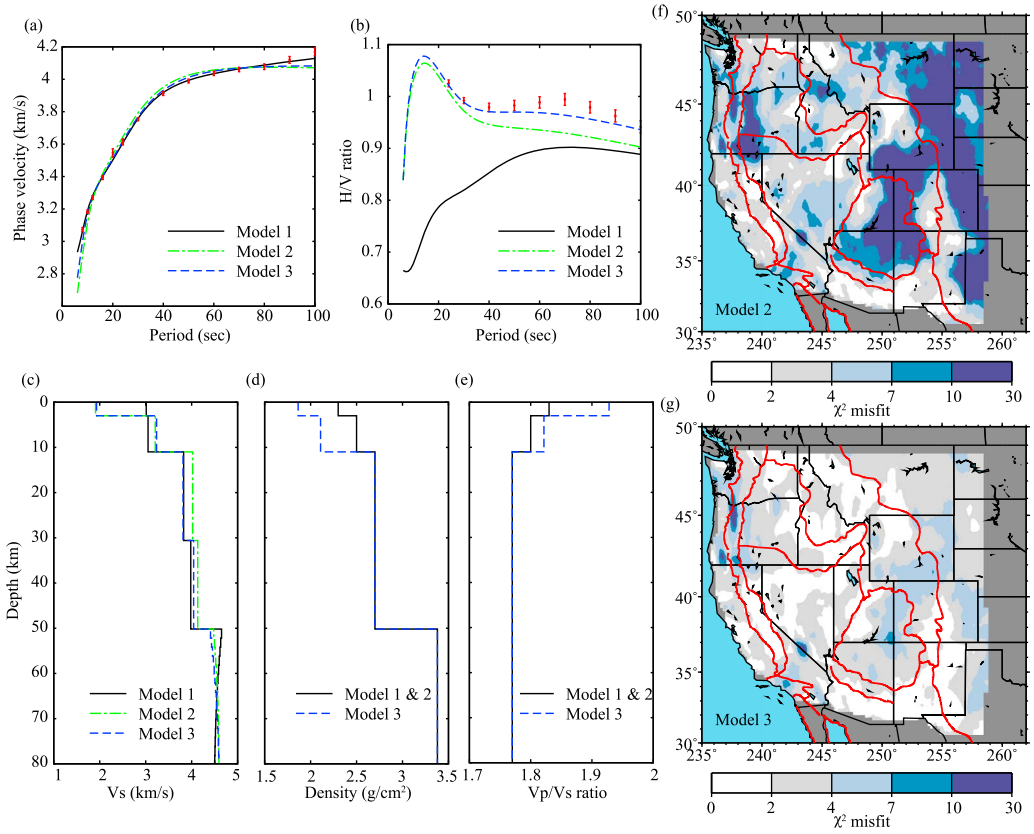

Figure 2. (a) Rayleigh wave phase velocity dispersion curves at a point in the Williston Basin (star in Figure 1a). The phase velocity measurements and their uncertainties are shown as red bars. The dispersion curves predicted based on Model 1, 2, and 3 shown in Figures 2c–2e are shown as black solid line, green dot-dash line, and blue dash line, respectively. (b) Same as Figure 2a but for Rayleigh wave H/V ratio. (c) The inverted 1D Vs profiles. The 1D profiles from Model 1, 2, and 3 are shown as black solid line, green dot-dash line, and blue dash line, respectively. (d, e) The reference 1D density and Vp/Vs ratio profile in Model 1 and 2 (solid black) and the inverted profiles in Model 3 (dash blue). (f) The overall χ^2 misfit in Model 2. (g) Same as Figure 2f but for Model 3.

sufficient to simultaneously satisfy both datasets. Figure 2f summarizes the overall misfit across the whole western U.S. for Model 2. Significant misfit ($\chi^2 > 10$) is observed in areas characterized by high H/V ratio (Figures 1a and 1b), which are mostly located in major sedimentary basins. In addition to low Vs, low density and high Vp/Vs ratio are also likely in sedimentary basins, particularly if there is a poorly consolidated layer [*Mavko et al.*, 1998; *Brocher*, 2005] and the corresponding effects on phase velocity and H/V ratios may not be negligible (see the example sensitivity kernels shown in Figure 1).

[12] In the inversion for Model 3, we allow density and Vp/Vs to vary in the top two crustal layers and is otherwise like Model 2. Due to the tradeoff between density and Vp/Vs ratio (see discussion in Section 3), a somewhat artificial damping function $f(\mathbf{m})$,

$$f(\mathbf{m}) = \sum_i \left\{ \left| \frac{Vs - Vs_2}{0.15 \cdot Vs_2} \right|^2 + \left| \frac{\rho - \rho_2}{0.15 \cdot \rho_2} \right|^2 + \left| \frac{Vp/Vs - (Vp/Vs)_2}{0.075 \cdot (Vp/Vs)_2} \right|^2 \right\}_i,$$

is added to the overall misfit ($\chi^2 = (\chi_c^2 + \chi_{H/V}^2) / 2$) to stabilize the inversion, where Vs_2, ρ_2, and $(Vp/Vs)_2$ are the model parameters taken from Model 2 and i denotes the summation over parameters in different layers and B-splines. Despite the damping function being somewhat arbitrary, our results are relatively robust to small changes in damping parameters. The need for damping could be replaced by an ad hoc empirical relationship between Vs, Vp, and density [e.g., *Brocher*, 2005; *Yano et al.*, 2009]. However, although such an approach could be attractive in a more uniform geological setting, it would oversimplify the complexity of upper crustal variations across the entire western US. Moreover, data sensitivity and tradeoffs can be better studied by not choosing an ad hoc functional form between different model parameters. We therefore choose the *f(m)* damping and do not use any empirical scalings.

[13] At the example location, a lower density and higher Vp/Vs ratio in the uppermost crust is observed compared to the reference model (Figures 2c–2e) and the H/V ratio can now be better predicted (Figure 2b). This is again consistent with having a ~3 km slow Vs sedimentary layer on the top. Tests based on different model parameterizations and damping regularizations suggest that while the relatively low density in the second crustal layer (3–11 km) can be caused by unaccounted for shallower or deeper density and Vp/Vs variations, the low density and high Vp/Vs ratio in the uppermost crust (0–3 km) is a robust feature. Figure 2g summarizes the overall misfit across the whole area based on Model 3. Significant misfit reduction is observed compared to Model 2 (Figure 2f) where most areas now have χ^2

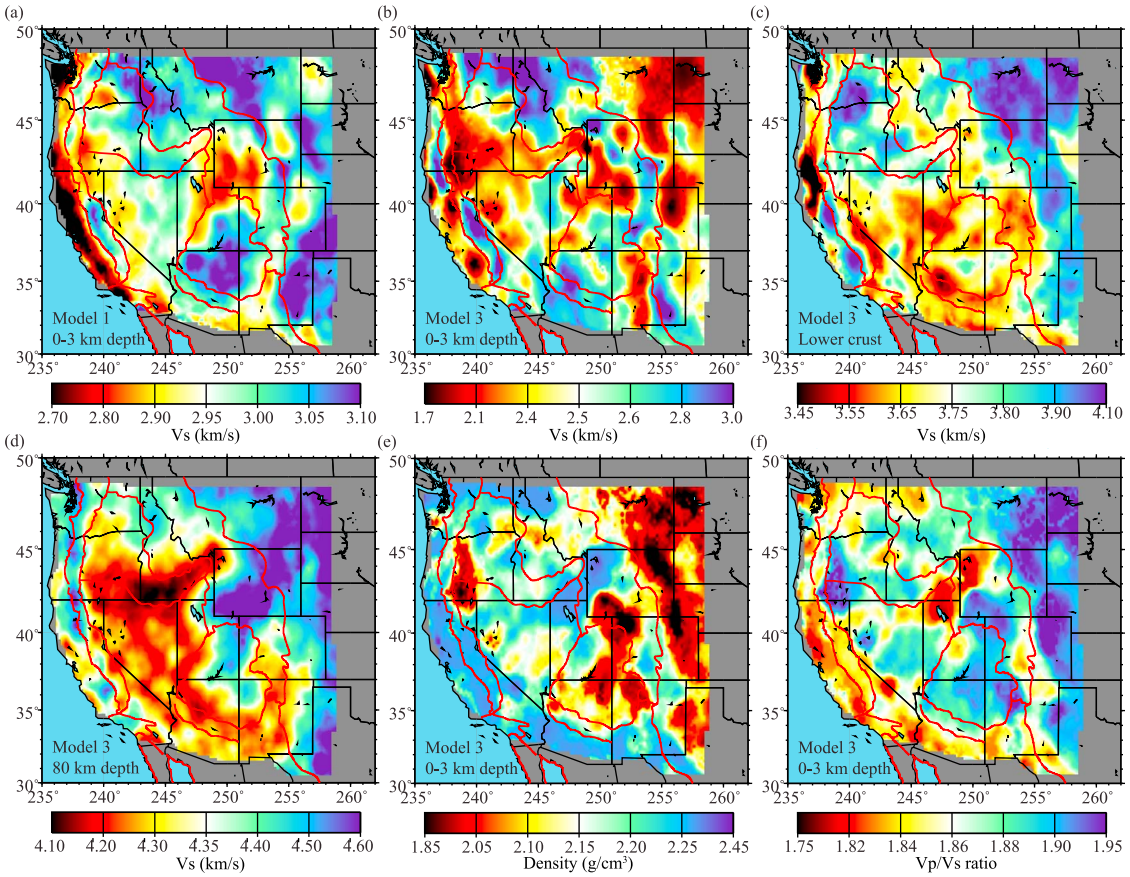

Figure 3. (a) The invert Vs in the uppermost crustal layer (0–3 km) in Model 1. (b) Same as Figure 3a but for Model 3. Note the color scales are different in Figures 3a and 3b. (c, d) Same as Figure 3b but for the bottom crustal layer and at 80 km depth. (e, f) The inverted density and Vp/Vs ratio in the uppermost crustal layer in Model 3.

misfit smaller than 4. Note that except for the uppermost crustal layer, the Vs profile is well constrained with phase velocity measurements alone and only small differences are observed between Models 1, 2, and 3 (e.g., Figure 2c).

[14] Figures 3b, 3e, and 3f summarize the Vs, density, and Vp/Vs of the uppermost crustal layer in Model 3 where the Vs in the bottom crustal layer and at 80 km depth are also shown in Figures 3c and 3d for reference. Clear differences are observed in the uppermost crustal Vs structure between Model 1 and Model 3 (Figures 3a and 3b; note the color bar differences between Figures 3a and 3b). In Model 3, which is our preferred model, pronounced slow anomalies in the top crustal layer with Vs < 2.5 km/s are observed in all major sedimentary basins such as the Williston Basin, the Green River Basin, the Denver Basin, the Powder River Basin, and the Central Valley. Besides the Central Valley in California, low density (<2.1 g/cm^3) and high Vp/Vs ratio (>1.9) are also observed in these basins likely due to weakly consolidated sediments near the surface. Note that most TA stations deployed nearby the Central Valley are located on the edge of the valley. While traveltime measurements based on wave propagation are sensitive to the slow interior of the basin, our results indicate that the sensitivity of the H/V ratio measurements is more localized beneath the station. When station distribution does not match the structural variations, phase velocity and H/V ratio measurements may not be completely compatible.

[15] Despite the overall misfit improvement when we allow density and the Vp/Vs ratio to change in the top two layers (Figures 2f and 2g), small discrepancies are still observed between the predicted and observed H/V ratios at long periods (e.g., Figure 2b), particularly in areas characterized by high velocity lower crust and upper mantle (Figures 2g, 3c, and 3d). This suggests that further model perturbations are needed. Investigating deeper density and Vp/Vs structure is, however, beyond the scope of this study and will be the subject of future contributions.

3. Discussion

[16] In the previous section, we demonstrate that Rayleigh wave phase velocity measurements between 8 and 100 sec period and H/V ratio measurements between 24 and 100 sec period are generally compatible and can be explained by the jointly inverted 3D model. The uppermost crustal model (0–3 km), in particular, is better constrained when the H/V ratio measurements are included as constraints. Clear correlation can be observed between the inverted uppermost crustal Vs model and geologic features at the surface, with pronounced slow anomalies observed in major sedimentary basins.

[17] Moreover, we show that not only Vs but also variations in density and the Vp/Vs ratio in the uppermost crust are necessary to explain both phase velocity and H/V ratio observations. There is, however, a strong tradeoff between

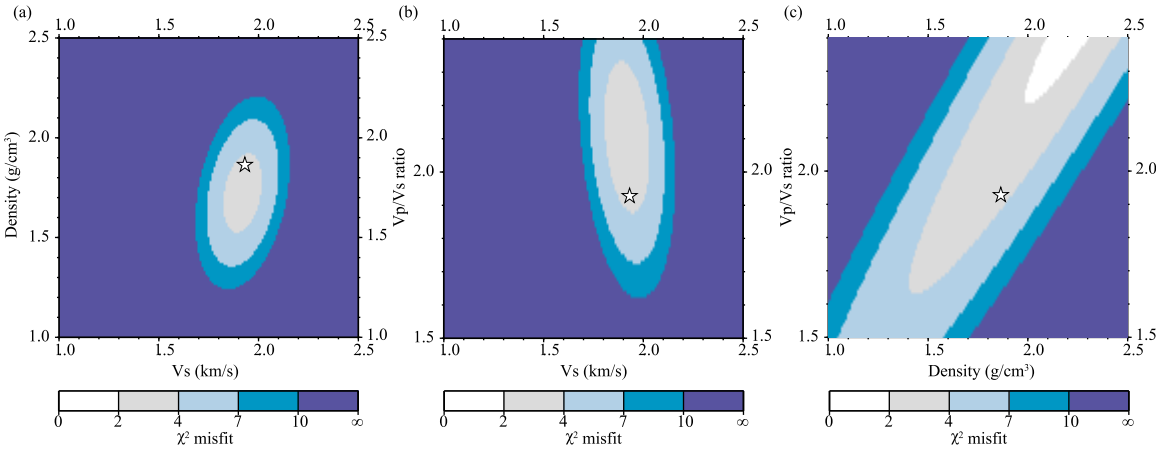

Figure 4. (a) The overall misfit surface at the example location (star in Figure 1a) when Vs and density are perturbed near Model 3. The star denotes the Vs and density in Model 3, which is different from the minimum misfit location due to the damping regularization applied in the inversion. (b, c) Same as Figure 4a but when Vs and Vp/Vs ratio and density and Vp/Vs ratio are perturbed.

density and Vp/Vs, which prevents them from being constrained without damping regularization. Figure 4 shows the overall misfit χ^2 when Vs, density, and Vp/Vs ratio in the uppermost crustal layer are perturbed in Model 3 at the example location in the Williston Basin. Relatively weak tradeoffs are observed between Vs and the other two parameters, where Vs is mostly ranging between 1.8–2.0 km/s if we consider $\chi^2 < 4$ as the acceptable criterion (Figures 4a and 4b). A strong tradeoff, on the other hand, is observed between density and the Vp/Vs ratio (Figure 4c). Models with high Vp/Vs ratio require high density and vice versa to fit the data. Again, this tradeoff could potentially be diminished by considering empirical relationships between crustal properties [e.g., *Brocher*, 2005], which indicate that both high density and high Vp/Vs ratio and low density and low Vp/Vs ratio can be ruled out for a sedimentary layer.

[18] In the back-arc region of Oregon and northernmost California we find Vs in the upper 3 km similar to that in basins with a sedimentary thickness of ≥3 km according to the compilation of *Blackwell et al.* [2006], though the actual sedimentary thickness in most of this region is not well constrained. A seismic refraction experiment on the Modoc Plateau at the southern end of the slow Vs feature found Vp of 2.1–4.4 km/s extending to 4.5 km depth and attributed it to volcanically derived sediments [*Fuis et al.*, 1987]. This is consistent with the results presented here, and hence we suggest that a similar uppermost crustal layer likely extends northward in the Oregon Cascades back-arc.

[19] Besides Rayleigh wave phase velocity and H/V ratio measurements, recently Lin et al. 2012 also demonstrated that a third Rayleigh wave quantity called local amplification can be measured across USArray. The local amplification, which describes how surface wave amplitude is affected by subsurface structures, is particularly sensitive to shallow Vp/Vs ratios [*Lin et al.*, 2012]. While Love wave measurements are also sensitive to shallow structure and can provide additional constraints, radial anisotropy must be accounted for when jointly inverting Rayleigh and Love wave measurements [*Moschetti et al.*, 2010]. Jointly inverting Rayleigh wave phase velocity, H/V ratio, and local amplification measurements for Vs, density, and Vp/Vs ratio in the crust and upper mantle will be a natural extension of this study.

[20] **Acknowledgments.** Instruments (data) used in this study were made available through EarthScope (EAR-0323309), supported by the National Science Foundation. The facilities of the IRIS Data Management System (EAR-0552316) were used for access the waveform and metadata required in this study. The authors are grateful to Donald Forsyth and an anonymous reviewer for comments that helped to improve this paper. This research was supported by the Director's Post-Doctoral Fellowship of the Seismological Laboratory at the California Institute of Technology and the Gordon and Betty Moore Foundation.

[21] The Editor thanks the two anonymous reviewers for assisting in the evaluation of this paper.

References

Bensen, G. D., M. H. Ritzwoller, M. P. Barmin, A. L. Levshin, F. Lin, M. P. Moschetti, N. M. Shapiro, and Y. Yang (2007), Processing seismic ambient noise data to obtain reliable broad-band surface wave dispersion measurements, *Geophys. J. Int.*, *169*, 1239–1260, doi:10.1111/j.1365-246X.2007.03374.x.

Blackwell, D. D., P. T. Negraru, and M. C. Richards (2006), Assessment of the enhanced geothermal system resource base of the United States, *Nat. Resour. Res.*, *15*(4), 283–308, doi:10.1007/s11053-007-9028-7.

Bonnefoy-Claudet, S., F. Cotton, and P.-Y. Bard (2006), The nature of the seismic noise wave field and its implication for site effects studies: A literature review, *Earth Sci. Rev.*, *79*(3–4), 205–227.

Boore, D., and M. Nafi Toksöz (1969), Rayleigh wave particle motion and crustal structure, *Bull. Seismol. Soc. Am.*, *59*, 331–346.

Bozdağ, E., and J. Trampert (2008), On crustal corrections in surface wave tomography, *Geophys. J. Int.*, *172*, 1066–1082, doi:10.1111/j.1365-246X.2007.03690.x.

Brocher, T. (2005), Empirical relations between elastic wavespeeds and density in the Earth's crust, *Bull. Seismol. Soc. Am.*, *95*(6), 2081–2092, doi:10.1785/0120050077.

Dziewonski, A. M., and D. L. Anderson (1981), Preliminary reference Earth model, *Phys. Earth Planet. Inter.*, *25*, 297–356, doi:10.1016/0031-9201(81)90046-7.

Fäh, D., F. Kind, and D. Giardini (2001), A theoretical investigation of average *H/V* ratios, *Geophys. J. Int.*, *145*, 535–549, doi:10.1046/j.0956-540x.2001.01406.x.

Ferreira, A. M. G., and J. H. Woodhouse (2007), Observations of long period Rayleigh wave ellipticity, *Geophys. J. Int.*, *169*, 161–169, doi:10.1111/j.1365-246X.2006.03276.x.

Fuis, G. S., J. J. Zucca, W. D. Mooney, and B. Milkereit (1987), A geologic interpretation of seismic-refraction results in northeastern California, *Geol. Soc. Am. Bull.*, *98*, 53–65, doi:10.1130/0016-7606(1987)98<53:AGIOSR>2.0.CO;2.

Gerhard, L. C., S. B. Anderson, J. A. LeFever, and C. G. Carlson (1982), Geological development, origin, and energy mineral resources of Williston Basin, North Dakota, *AAPG Bull.*, *66*, 989–1020.

Hajnal, Z., C. M. R. Fowler, R. F. Mereu, E. R. Kanasewich, G. L. Cunmiing, A. G. Green, and A. Mair (1984), An initial analysis of the earth's crust under the Williston basis: 1979 COCRUST experiment, *J. Geophys. Res.*, *89*(B11), 9381–9400, doi:10.1029/JB089iB11p09381.

Herrmann, R. B., and C. J. Ammon (2002), *Computer Programs in Seismology: Surface Waves, Receiver Functions and Crustal Structure*, St. Louis Univ., St. Louis, Mo.

Langston, C. A. (2011), Wavefield continuation and decomposition for passive seismic imaging under deep unconsolidated sediments, *Bull. Seismol. Soc. Am.*, *101*(5), 2176–2190, doi:10.1785/0120100299.

Lin, F., and M. H. Ritzwoller (2011), Helmholtz surface wave tomography for isotropic and azimuthally anisotropic structure, *Geophys. J. Int.*, *186*, 1104–1120, doi:10.1111/j.1365-246X.2011.05070.x.

Lin, F., M. H. Ritzwoller, and R. Snieder (2009), Eikonal tomography: Surface wave tomography by phase front tracking across a regional broadband seismic array, *Geophys. J. Int.*, *177*(3), 1091–1110, doi:10.1111/j.1365-246X.2009.04105.x.

Lin, F., M. H. Ritzwoller, Y. Yang, M. P. Moschetti, and M. J. Fouch (2011), Complex and variable crustal and uppermost mantle seismic anisotropy in the western United States, *Nat. Geosci.*, *4*, 55–61, doi:10.1038/ngeo1036.

Lin, F. C., V. Tsai, and M. H. Ritzwoller (2012), The local amplification of surface waves: A new observable to constrain elastic velocities, density, and anelastic attenuation, *J. Geophys. Res.*, doi:10.1029/2012JB009208, in press.

Mavko, G., T. Mukerji, and J. Dvorkin (1998), *The Rock Physics Handbook: Tools for Seismic Analysis in Porous Media*, 329 pp., Cambridge Univ. Press, Cambridge, U. K.

Morel-a-l'Huissier, P., A. G. Green, and C. J. Pike (1987), Crustal refraction surveys across the Trans-Hudson Orogen/Williston Basin of south central Canada, *J. Geophys. Res.*, *92*(B7), 6403–6420, doi:10.1029/JB092iB07p06403.

Moschetti, M. P., M. H. Ritzwoller, F.-C. Lin, and Y. Yang (2010), Crustal shear wave velocity structure of the western United States inferred from ambient seismic noise and earthquake data, *J. Geophys. Res.*, *115*, B10306, doi:10.1029/2010JB007448.

Nakamura, Y. (1989), A method for dynamic characteristics estimation of subsurface using microtremor on the ground surface, *Q. Rep. Railw. Tech. Res. Inst.*, *30*, 25–30.

Pollitz, F. F., and J. A. Snoke (2010), Rayleigh-wave phase-velocity maps and three-dimensional shear velocity structure of the western US from local non-plane surface wave tomography, *Geophys. J. Int.*, *180*, 1153–1169, doi:10.1111/j.1365-246X.2009.04441.x.

Spikes, K. T. (2011), Modeling elastic properties and assessing uncertainty of fracture parameters in the Middle Bakken Siltstone, *Geophysics*, *76*(4), E117–E126, doi:10.1190/1.3581129.

Tanimoto, T., and L. Rivera (2008), The ZH ratio method for long-period seismic data: Sensitivity kernels and observational techniques, *Geophys. J. Int.*, *172*, 187–198, doi:10.1111/j.1365-246X.2007.03609.x.

Vidale, J. E., and D. V. Helmberger (1988), Elastic finite-difference modeling of the 1971 San Fernando, California earthquake, *Bull. Seismol. Soc. Am.*, *78*, 122–141.

Waldhauser, F., R. Lippitsch, E. Kissling, and J. Ansorge (2002), High-resolution teleseismic tomography of upper-mantle structure using an *a priori* three-dimensional crustal model, *Geophys. J. Int.*, *150*, 403–414, doi:10.1046/j.1365-246X.2002.01690.x.

Yang, Y., M. H. Ritzwoller, and C. H. Jones (2011), Crustal structure determined from ambient noise tomography near the magmatic centers of the Coso region, southeastern California, *Geochem. Geophys. Geosyst.*, *12*, Q02009, doi:10.1029/2010GC003362.

Yano, T., T. Tanimoto, and L. Rivera (2009), The ZH ratio method for long-period seismic data: inversion for *S*-wave velocity structure, *Geophys. J. Int.*, *179*, 413–424, doi:10.1111/j.1365-246X.2009.04293.x.